Supporting Information

All-self-metered solution-coating process in ambient air for the fabrication of efficient, large-area, and semitransparent perovskite solar cells

*In-Gon Bae and Byoungchoo Park**

Department of Electrophysics, Kwangwoon University, Wolgye-Dong, Seoul 01897, Korea
* bcpark@kw.ac.kr

Experimental

Materials

All materials here were purchased from commercial sources and were used without any further purification. Nickel(II) nitrate hexahydrate ($Ni(NO_3)_2 \cdot 6H_2O$), poly(oxyethylene tridecyl ether) (PTE), gamma-butyrolactone (GBL, 99%), anhydrous dimethyl sulfoxide (DMSO, 99.9%), and anhydrous chlorobenzene (CB, 99.9%) were purchased from Sigma-Aldrich. Isopropyl alcohol (IPA, 99.7%) was purchased from Daejung. Lead(II)iodide (PbI_2, 99.9985%) was purchased Alfa Aesar, and methyl-ammonium iodide (CH_3NH_3I, MAI) was purchased from Dyesol. Phenyl-C_{61}-butyric acid methyl ester (PCBM) was purchased from Nano-C. The suspensions of ZnO nanoparticles (NPs) (N-10) and SnO_2 NPs (N-31) used in this study were purchased from Avantama and were dispersed in IPA and butanol, respectively. Bathocuproine (BCP, 98%) was purchased from TCI. In order to fabricate the semitransparent electrode, we purchased a silver nanowire (AgNW) suspension dispersed in IPA (0.5–2.0 wt%, NTC-01) from Nanopyxis Co., Ltd.

Horizontal dip-coating technique

Functional layers were coated onto the substrates using a self-metered horizontal-dip-coater (H-dip-coater) according to the following process: a small amount of the solution (5~25 μl) per unit of coating area (1 cm^2) was fed into the gap of the cylindrical barrier using a syringe pump (NE-1000, New Era Pump Systems Inc.).[1] The gap height h_0 was adjusted vertically using

micrometer positioners mounted at the end of the coating barrier, and the coating speed *U* was controlled using a computer-controlled translation stage (SGSP26-200, Sigma Koki Co., Ltd). After a concave meniscus of the coating solution had formed on the substrate, the substrate was transported horizontally such that the meniscus formed by the coating barrier caused the solution to spread evenly on the transporting substrate while maintaining the shape of the meniscus of the solution on the substrate.

Perovskite solar cell fabrication

A patterned indium-tin-oxide (ITO) layer (80 nm, 30 ohm/square) on a glass substrate was used as a transparent anode. The ITO/glass substrate was cleaned with detergent, deionised water, acetone, and IPA, and then dried by blowing nitrogen over it, followed by ultra-violet ozone cleaning for 5 min. All functional layers on the patterned ITO/glass substrates were fabricated by the self-metered H-dip-coating technique. To coat the ITO/glass substrate with a NiO hole-collecting layer, nickel(II) nitrate hexahydrate was dissolved in IPA (8.5 wt%), and this solution was then coated using the H-dip-coating technique onto substrates pre-heated to 60 °C. The coating speed was 1.2 cm/s at h_0 = 0.30 mm. Afterward, the coated layer was annealed at 300 °C for one hour.[2] For the perovskite layer, a precursor solution was prepared by mixing 3 mmol of PbI_2 and MAI at a molar ratio of 1:1 in GBL and DMSO at 7:3 vol with an addition of poly(oxyethylene tridecyl ether) (PTE) as a surfactant additive (10 ppm) followed by stirring overnight at 70 °C. The precursor solution was filtrated with a PTFE syringe filter (0.2 μm, Whatman) and the solution (20 μl) was then H-dip-coated onto the NiO-coated substrates pre-heated to 120 °C in air with a coating speed of 0.8 - 4.0 cm/s without any gas quenching and/or anti-solvent treatment process to form uniform perovskite films (250 nm). For a PCBM electron-collecting coating layer (50 nm), PCBM was dissolved in CB, and this solution was then H-dip-coated onto the $MAPbI_3$ perovskite layer at 60 °C at a coating speed of 2.0 cm/s. Subsequently, another electron injection layer of ZnO NPs (20 nm) was also H-dip-coated using the ZnO NP suspension on the underlying PCBM layer at room temperature at a coating speed of 2.0 cm/s.

Finally, a *ca.* 12-nm-thick BCP layer and an Al cathode (ca. 70 nm thick) layer were formed on the top of the ZnO layer via thermal deposition at a base pressure below 2.0×10^{-6} torr in a vacuum chamber. Thus, the layer structure of the fabricated device was ITO / NiO / $CH_3NH_3PbI_3$ with PTE / PCBM / ZnO NPs / BCP / Al, and the active area of the device was 6 mm^2.

Semitransparent perovskite photovoltaic cell fabrication

The device structure of the semitransparent photovoltaic (PV) cell studied here was ITO / NiO / $CH_3NH_3PbI_3$ with PTE / PCBM / ZnO NPs / SnO_2 NPs / AgNW / ZnO NPs, with the layer structure identical to that of the PV cell mentioned above up to the electron injection layer of ZnO NPs. Thus, to form another 20-nm-thick electron transport layer of SnO_2, SnO_2 NPs were H-dip-coated using the SnO_2 NP suspension on the ZnO NPs layer. Next, in order to form a semitransparent electrode, AgNWs (~100 nm) were H-dip-coated using the AgNW suspension on the SnO_2 NPs layer. Finally, another 30-nm-thick ZnO NPs layer was formed on the AgNW semitransparent electrode in order to increase of connections among the AgNWs. To fabricate a large semitransparent perovskite PV cell,[3] all functional layers were H-dip-coated on a 13.0 cm × 13.0 cm substrate with an active area of 8.5 cm × 8.5 cm.

Film and device characterisation

The surface morphologies of the functional layers fabricated were investigated by scanning electron microscopy (SEM, JSM-6700F, JEOL Co.). In order to investigate the microscale roughness and surface potential of the functional layers, non-contact atomic force microscopy (AFM) and simultaneous Kelvin probe force microscopy (KPFM, FlexAFM, Nanosurf AG) were used by applying an AC voltage of 1 V at a frequency of 18 kHz to a Pt/Ir-coated silicon tip (resonance frequency = 87 kHz and force constant = 3.9 N/m, NanoWorld, Inc.). The crystallinity of the fabricated perovskite layer was evaluated using an X-ray diffractometer (XRD-Rigaku D/max 2200, λ= 0.154 nm). The optical absorption spectra of the layer were also investigated using a UV-visible spectroscopy system (8453, Agilent). The photoluminescence

(PL) spectra of the functional layer were recorded using a fluorescence spectrophotometer (Cary Eclipse Fluorescence Spectrophotometer, Agilent). The device performance of the PV cells was measured using a source meter (2400, Keithley) and was calibrated using a reference cell (BS-520, Bunkoh-Keiki) under illumination of 100 mW/cm^2 produced by an AM 1.5G light source (96000 Solar Simulator, Newport). The external and internal quantum efficiency (EQE and IQE) spectra were also obtained using a measurement system (IQE-200 EQE/ IQE, Newport). In order to measure the PV performance of the large size perovskite PV cell, we used photo-masks with an aperture size of 0.08 cm^2.

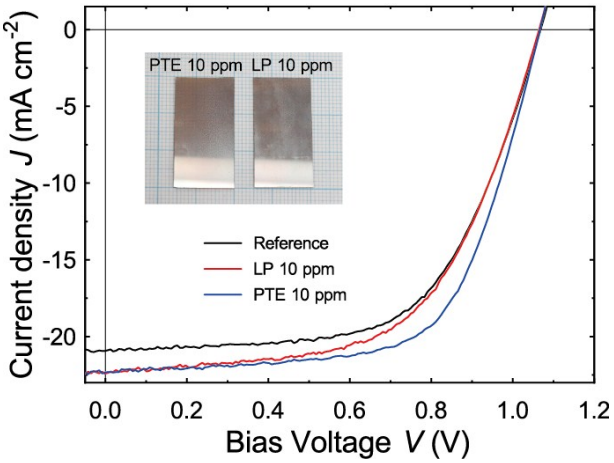

Figure S1 Photo *J-V* curves of the H-dip-coated $MAPbI_3$ perovskite PV cells without (reference) and with surfactant additives of PTE (10 ppm) or LP (10 ppm) under AM 1.5 G illumination. The inset shows a photographic image of perovskite layers fabricated by the H-dip-coating method with the surfactant additives of PTE (left) or LP (right).

Table S1. Summary of the PV performances of H-dip-coated $MAPbI_3$ perovskite PV cells with the PTE and LP surfactant additives for several surfactant concentrations

Surfactant / concentration		V_{oc} (V)	J_{sc} (mA/cm^2)	*FF* (%)	PCE (%)
PTE	5.0 ppm	1.05 ± 0.02	22.73 ± 0.17	58.19 ± 2.51	13.89 ± 0.75
	7.5 ppm	1.05 ± 0.01	21.13 ± 0.20	61.86 ± 1.86	13.77 ± 0.35
	10.0 ppm	1.07 ± 0.00	22.36 ± 0.45	64.83 ± 0.43	15.46 ± 0.14
	12.5 ppm	1.07 ± 0.00	21.91 ± 0.05	61.73 ± 2.05	14.43 ± 0.57
	20.0 ppm	1.05 ± 0.00	23.37 ± 0.15	58.27 ± 0.01	14.30 ± 0.09
	0.03 wt%	1.06 ± 0.01	19.30 ± 0.25	65.32 ± 2.27	13.38 ± 0.20
	0.07 wt%	1.10 ± 0.02	18.36 ± 0.30	34.53 ± 2.69	13.00 ± 0.23

	0.11 wt%	1.06 ± 0.01	17.80 ± 0.28	63.60 ± 2.55	12.02 ± 0.19
LP	5.0 ppm	1.07 ± 0.01	20.85 ± 0.48	13.53 ± 0.30	13.53 ± 0.30
	7.5 ppm	1.06 ± 0.00	21.01 ± 0.62	61.57 ± 1.54	13.76 ± 0.22
	10.0 ppm	1.06 ± 0.00	22.42 ± 0.36	58.47 ± 0.39	13.94 ± 0.13
	12.5 ppm	1.04 ± 0.00	22.18 ± 0.04	57.47 ± 0.41	13.29 ± 0.07
	20.0 ppm	1.03 ± 0.00	21.70 ± 0.03	59.43 ± 1.14	13.23 ± 0.17

(All data were averaged for four pixels.)

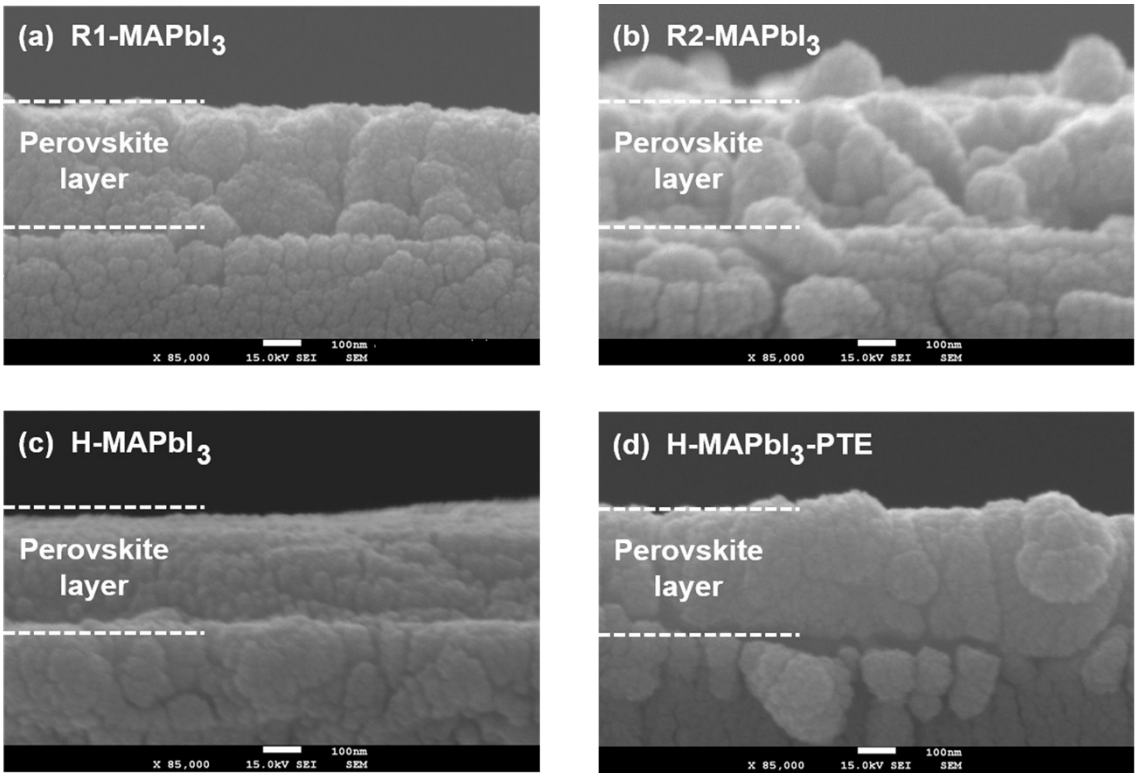

Fig. S2 High-magnification (× 85,000) cross-sectional SEM images of four $MAPbI_3$ perovskite layers: R1-$MAPbI_3$ (a), R2-$MAPbI_3$ (b), H-$MAPbI_3$ (c), and H-$MAPbI_3$-PTE (d).

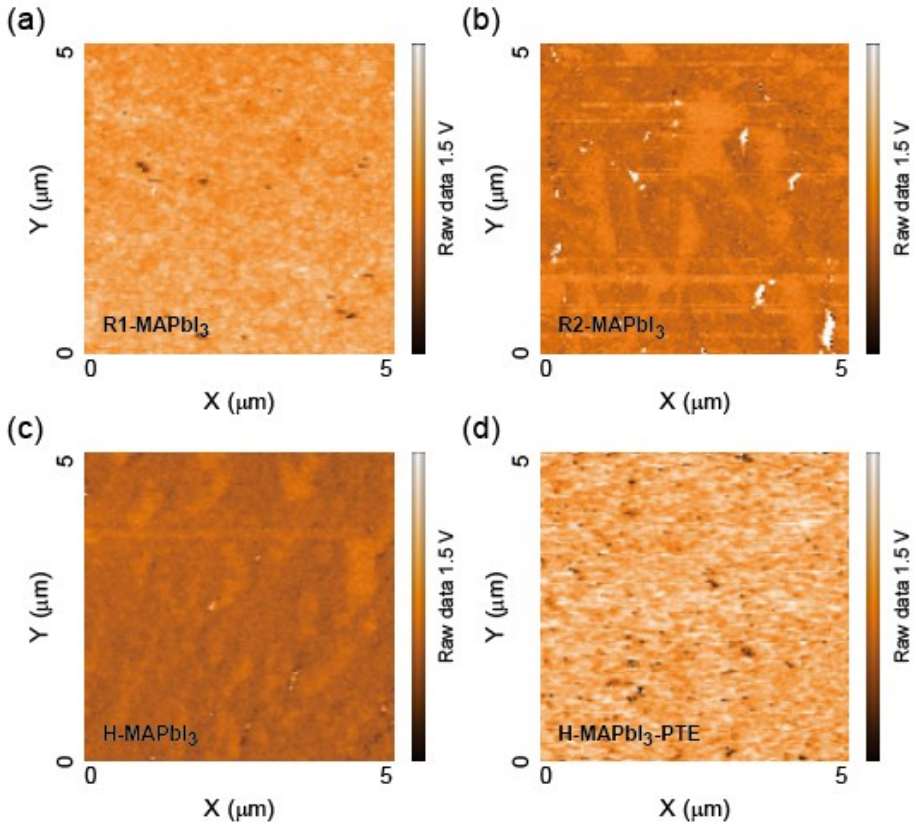

Fig. S3 KPFM surface potential maps of the investigated perovskite layers: (a) R1-$MAPbI_3$, (b) R2-$MAPbI_3$, (c) H-$MAPbI_3$ and (d) H-$MAPbI_3$-PTE.

In order to investigate the energy-level characteristics of the fabricated perovskite layers, we monitored the surface potentials of the perovskite layers using a KPFM (Fig. S3). Figure S3a presents a KPFM map (5 μm × 5 μm) of the reference layer of R1-$MAPbI_3$. This figure shows a fairly flat surface potential map with an average value close to 0.49 V. Using this surface potential, we can obtain the Fermi level of R1-$MAPbI_3$ through a comparison with the surface potential of a standard surface of highly oriented pyrolytic graphite (HOPG, ZYB, Optigraph GmbH).[S4] The estimated Fermi level of R1-$MAPbI_3$ is about 4.97 eV, similar to the Fermi level (~4.8-5.0 eV) of a representative $MAPbI_3$ perovskite layer, as reported previously.[S5] In contrast, the surface potential of R2-$MAPbI_3$ prepared by the spin-coating method in air exhibits a very rough surface potential map (Fig. S3b) with an average surface potential of 0.23 V, resulting in a Fermi level of approximately 5.23 eV, likely due to the formation of needle-like defects. Meanwhile, as shown in Fig. S3c, the surface potential map of H-$MAPbI_3$ shows clearly different aspects from those of R2-$MAPbI_3$. Despite the fact that H-$MAPbI_3$ was fabricated in an air atmosphere, it shows a relatively smooth surface potential map with an average surface potential value of 0.37 V (and a Fermi level of 5.09 eV) due to the formation of large-sized grains (Fig. 3c), as mentioned in the manuscript. Moreover, as shown in Fig. S3d, the surface potential of H-$MAPbI_3$-PTE also shows a very smooth potential map with an average surface potential value of 0.52 V and a Fermi level of 4.94 eV, values which are quite similar to those of R1-$MAPbI_3$. Thus, it is clear that the homogeneous H-dip-coated $MAPbI_3$ perovskite layer with PTE exhibits energy-level characteristics nearly identical to those of the spin-coated $MAPbI_3$ perovskite layer fabricated with N_2 in spite of the use of an air fabrication process.

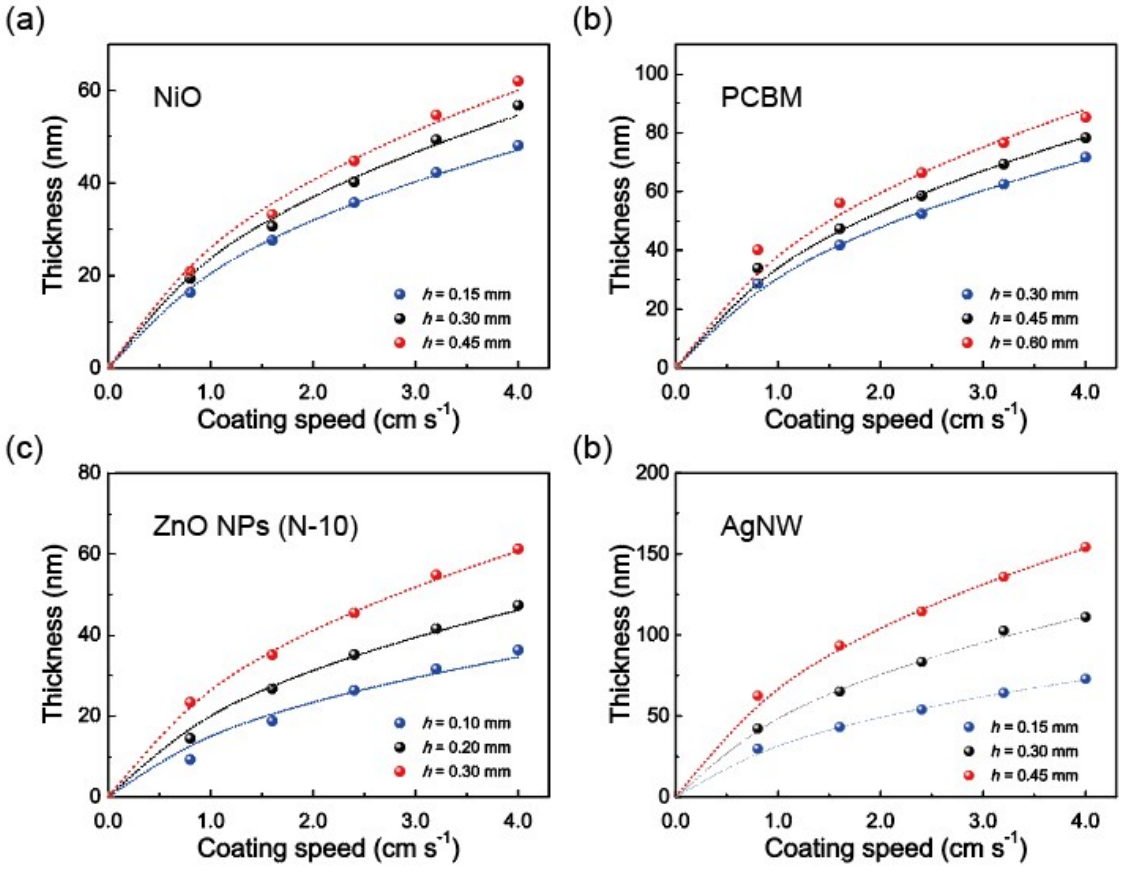

Fig. S4 Film thickness data of the H-dip-coated functional layers of hole-collecting NiO (a), electron-collecting PCBM (b), electron-transporting ZnO NPs (c), and conducting AgNWs (d) as a function of the coating speed U for three gap heights, h_0. The dotted curves show the theoretically fitted predictions according to the Landau–Levich equation.

We measured the film thickness (h) of the H-dip-coated NiO, PCBM, ZnO NP, and AgNW layers as a function of the coating speed U for three gap heights with the Landau-Levich menisci of their suspensions (Fig. S4). It is clear from the figure that for a given h_0, the thicknesses of the all-H-dip-coated layers of NiO, PCBM, ZnO NPs, and AgNWs showed continuous increases with an increase in U. These results were in good agreement with the associated drag-out problem, as shown in the figures.

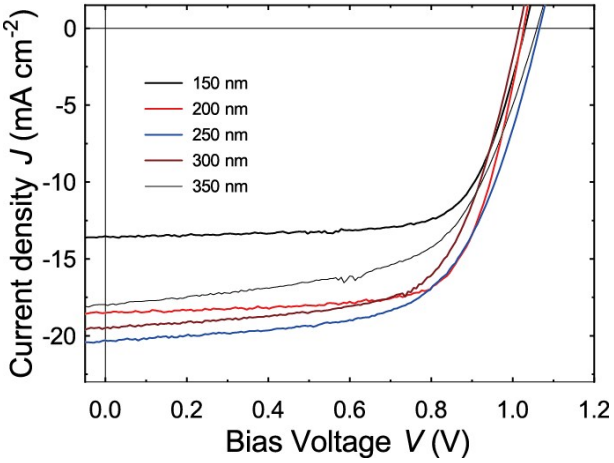

Figure S5 Photo *J-V* characteristics of five perovskite solar cells using an H-dip-coated $MAPbI_3$ PV layer with the PTE surfactant (10 ppm) for several thicknesses of H-dip-coated $MAPbI_3$ PV layers under AM 1.5 G illumination.

Table S2. Summary of the PV performances of perovskite solar cells using the H-dip-coated $MAPbI_3$ PV layer with PTE surfactant additives (10 ppm) for several thicknesses of the PV layers under AM 1.5 G illumination

Thickness of PV layer (nm)	V_{oc} (V)	J_{sc} (mA/cm^2)	*FF* (%)	PCE (%)
150	1.02 ± 0.03	18.01 ± 0.41	70.20 ± 1.25	12.84 ± 0.38
200	1.04 ± 0.02	18.25 ± 0.25	71.59 ± 3.54	13.57 ± 0.37
250	1.05 ± 0.01	19.04 ± 0.90	70.82 ± 1.19	14.11 ± 0.68
300	1.04 ± 0.02	19.32 ± 1.07	63.85 ± 1.99	12.85 ± 0.39
350	1.06 ± 0.02	17.91 ± 1.36	57.35 ± 0.70	10.86 ± 1.07

(All data were averaged for four pixels.)

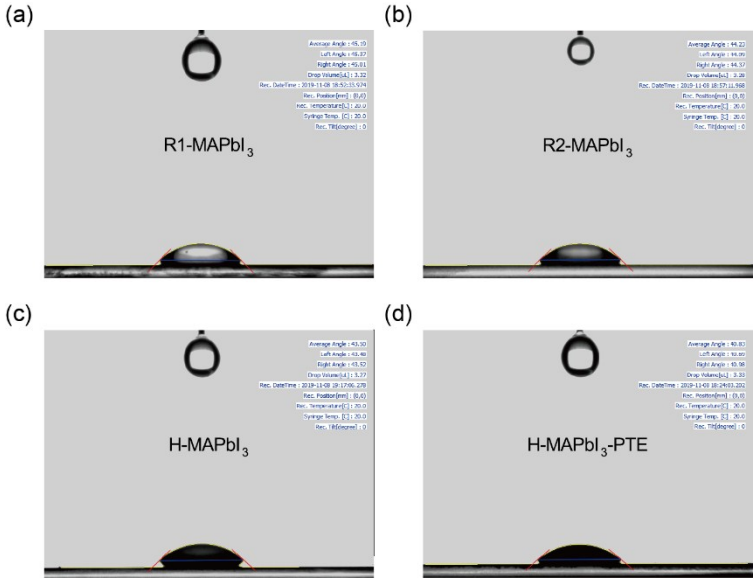

Figure S6 Contact angles of four $MAPbI_3$ layers for water droplets: (a) 45.2° for R1-$MAPbI_3$, (b) 44.2° for R2-$MAPbI_3$, (c) 43.5° for H-$MAPbI_3$, and (d) 40.8° for H-$MAPbI_3$-PTE.

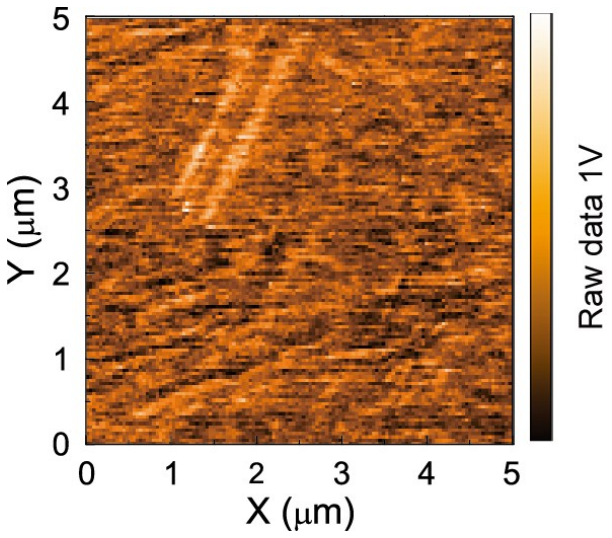

Figure S7 KPFM surface potential map of an H-dip-coated AgNW electrode. The estimated work function of the H-dip-coated AgNW electrode was approximately 4.64 eV.

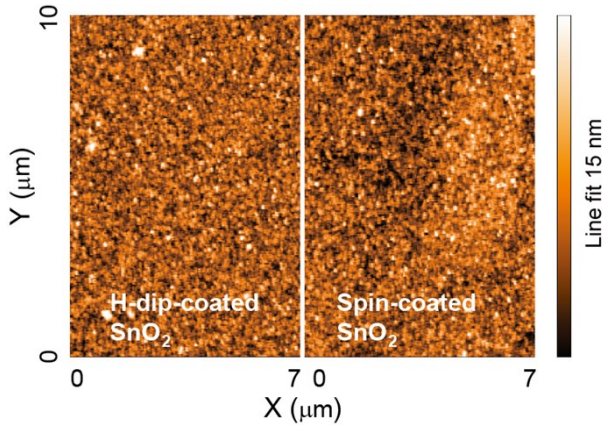

Figure S8 AFM topography images of the H-dip-coated and spin-coated SnO_2 layers with a layer thickness of 15 nm. The observed RMS surface roughness of the H-dip-coated SnO_2 layer was 1.85 nm, while the RMS surface roughness of the spin-coated SnO_2 layer was 2.01 nm.

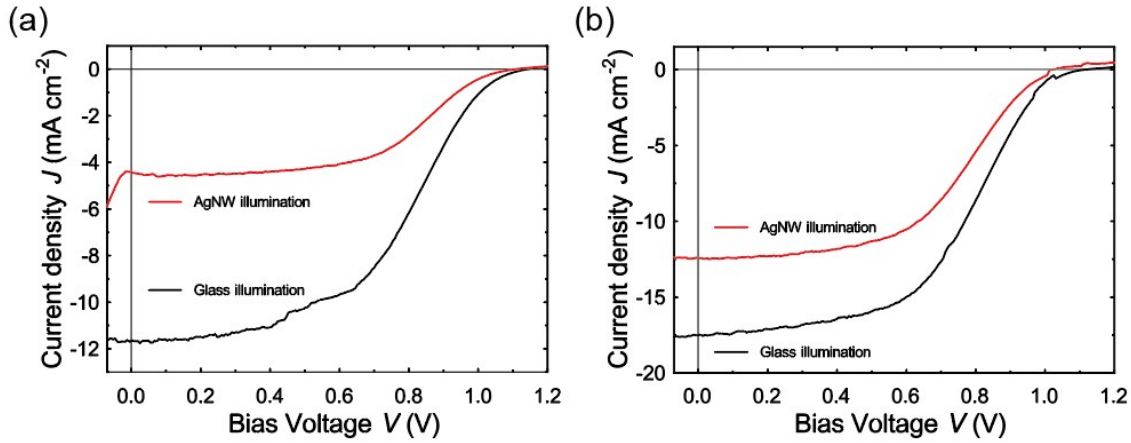

Fig. S9 Photo *J-V* characteristics of an H-dip coated perovskite solar cell with the H2 PV layer and a spin-coated AgNW cathode (a) and an H-dip coated perovskite solar cell with the H1 PV layer and a H-dip-coated AgNW cathode (b) under AM 1.5 G illumination.

Table S3. Summary of the PV performances of the H-dip-coated semitransparent perovskite solar cells with the H2 PV layer and spin-coated AgNW cathode under AM 1.5 G illumination

Illumination	V_{oc} (V)	J_{sc} (mA/cm^2)	*FF* (%)	PCE (%)
Glass side	1.14	11.60	53.58	6.07
AgNW side	1.11	4.57	59.79	2.60

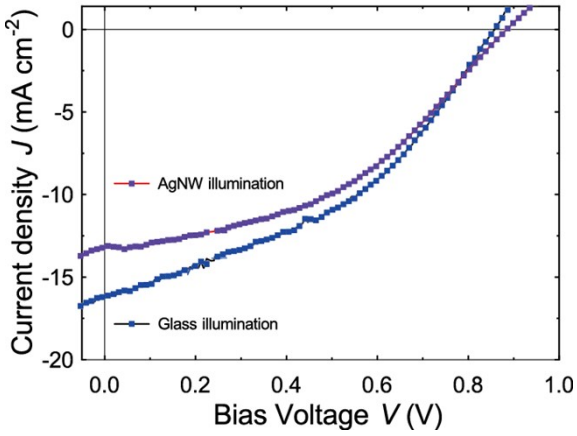

Figure S10 Photo *J-V* characteristics of a large-size semitransparent perovskite solar cell with an H-dip-coated $MAPbI_3$ PV layer with the PTE surfactant additive (10 ppm) under AM 1.5 G illumination.

Table S4. Summary of the PV performances of a large-size semitransparent perovskite solar cell with the H-dip-coated PV layer with the PTE surfactant additive (10 ppm) under AM 1.5 G illumination

Illumination	V_{oc} (V)	J_{sc} (mA/cm^2)	*FF* (%)	PCE (%)
Glass side	0.86	14.93	51.75	5.62
AgNW side	0.89	12.76	52.60	5.05

Table S5. Summary of the transmittance (*Tr*) over the wavelength range (λ nm) and PCE for recent small and large semitransparent solar cells with polymeric and inorganic PV layers

Major fabrication process	Device structure [Bottom electrode] / [PV layer (method)] / [Top electrode]	*Tr* [%] (λ nm)	PCE [%] (Active area [cm^2])	
			small	large
Vacuum-processing	[Al] / BSF / [DRIE[b]-c-Si (ion etching)] / emitter / Al_2O_3 / Si_3N_4 / [Al] (Ref. 4)	20 (400-750)	12.2 (1)	-
	[ITO] / PEDOT:PSS / [J52:IEICO-4F:$PC_{71}BM$ (spin in N_2)] / PFN-Br / [Ag] (Ref. 5)	15.8 (400-700)	8.8 (0.04)	-
	[ITO] / PEDOT:PSS / [PBDTTT-EFT:$PC_{70}BM$ (blade in air)] / MSAPBS[a] / [Al/Ag] (Ref. 6)	10 (380-800)	5 (0.04)	4.5 (216.0)
	[ITO] / PEDOT:PSS / [PBDTTT-EFT:$PC_{70}BM$ (blade in air)] / LiF / [Al/Ag] (Ref. 7)	10 (370-740)	5.6 (0.04)	5.3 (10.8)
Ambient air processing	[ITO] / ZnO / [P3HT:PCBM (spray in air)] / [PEDOT:PSS] (Ref. 8)	unknown	2.9 (0.3)	2.4 (4.0)
	[FTO] / ZnO / [PBTZT-stat-BDTT-8:$PC_{60}BM$ (slot-die in air)] / [PEDOT:PSS/AgNW] (Ref. 9)	10 (380-780)	5.2 (0.1)	4.8 (197.4)

[a]: 4,4′-(((methyl(4-sulphonatobutyl)ammonio)bis(propane-3,1-diyl))bis(dimethyl-ammoniumdiyl))bis-(butane-1-sulfonate)
[b]: Deep reactive ion etching

References

1. B. Park and M.-Y. Han, *Opt. Express*, 2009, **17**, 13830-13840.
2. X. Yin, Z. Yao, Q. Luo, X. Dai, Y. Zhou, Y. Zhang, Y. Zhou, S. Luo, J. Li, N. Wang and H. Lin, *ACS Appl. Mater. Interfaces*, 2017, **9**, 2439-2448.
3. Y. Deng, X. Zheng, Y. Bai, Q. Wang, J. Zhao and J. Huang, *Nat. Energy*, 2018, **3**, 560-566.
4. B. Park, J. N. Huh, W. S. Lee and I.-G. Bae, *J. Mater. Chem. C*, 2018, **6**, 2234-2244.
5. S. Olthof, *APL Mater.*, 2016, **4**, 091502.
6. K. Lee, N. Kim, K. Kim, H.-D. Um, W. Jin, D. Choi, J. Park, K. J. Park, S. Lee and K. Seo, *Joule*, 2020, **4**, 1-12.
7. H. Shi, R. Xia, G. Zhang, H.-L. Yip and Y. Cao, *Adv. Energy Mater.*, 2019, **9**, 1903438.
8. K.-M. Huang, Y. Q. Wong, M.-C. Lin, C.-H. Chen, C.-H. Liao, J.-Y. Chen, Y.-H. Huang, Y.-F. Chang, P.-T. Tsai, S.-H. Chen, C.-T. Liao, Y.-C. Lee, L. Hong, C.-Y. Chang, H.-F. Meng, Z. Ge, H.-W. Zan, S.-F. Horng, Y.-C. Chao and H. Y. Wong, *Prog. Photovolt. Res. Appl.*, 2019, **27**, 264-274.
9. Y. Q. Wong, H.-F. Meng, H. Y. Wong, C. S. Tan, C.-Y. Wu, P.-T. Tsai, C.-Y. Chang, S.-F. Horng and H.-W. Zan, *Org. Electron.*, 2017, **43**, 196-206.
10. Y.-C. Huang, C.-W. Chou, D.-H. Lu, C.-Y. Chen and C.-S. Tsao, *IEEE J. Photovolt.*, 2018, **8**, 144-150.
11. L. Lucera, F. Machui, H. D. Schmidt, T. Ahmad, P. Kubis, S. Strohm, J. Hepp, A. Vetter, H.-J. Egelhaaf and C. J. Brabec, *Org. Electron.*, 2017, **45**, 209-214.